A further experiment on two-dimensional decaying turbulence on a rotating sphere (*)(**)

S. YODEN [1], K. ISHIOKA [2], Y.-Y. HAYASHI [2][3] and M. YAMADA [2]

[1] *Department of Geophysics, Kyoto University, Kyoto, 606-8502, Japan*
[2] *Graduate School of Mathematical Sciences, University of Tokyo, Tokyo, 153-8914, Japan*
[3] *Division of Earth and Planetary Sciences, Hokkaido University, Sapporo, 060-0810, Japan*

(ricevuto il 18 Novembre 1998; revisionato il 27 Maggio 1999; approvato il 29 Giugno 1999)

Summary. — A series of numerical experiments on the two-dimensional decaying turbulence is performed for a non-divergent barotropic fluid on a rotating sphere by using a high-resolution spectral model. Time variations of the energy spectrum and the flow field are highly dependent on the rotation rate. In non-rotational cases, isolated coherent vortices emerge in the course of time development as in the planar two-dimensional turbulence. As the rotation rate increases, however, the evolution of the flow field changes drastically, and a westward circumpolar vortex appears in high-latitudes as well as zonal band structures in mid- and low-latitudes. The dependence of these features on the initial energy spectrum is investigated and the dynamics of such pattern formations is discussed.

PACS 92.60.Ek – Convection, turbulence, and diffusion.
PACS 47.54 – Pattern selection; pattern formation.
PACS 47.27.Eq – Turbulence simulation and modeling.
PACS 01.30.Cc – Conference proceedings.

1. – Introduction

In 1960s, the energy spectrum of k^{-3} in the enstrophy-cascading inertial subrange was theoretically predicted for the two-dimensional (2D) turbulence on an infinite plane [1-3]. Since then many numerical experiments have been done to investigate the nature of planar 2D turbulence, and nowadays high-resolution models with up to 4096^2 grids are available [4]. An interesting feature of the 2D turbulence is the emergence of isolated coherent vortices, which is due to a self-organizing mechanism involved in the disorder 2D motion [5].

As for an application to geophysical fluid, Rhines [6] firstly studied the 2D turbulence on a β-plane to investigate the effect of a rotating planet. His numerical

(*) Paper presented at the International Workshop on "Vortex Dynamics in Geophysical Flows", Castro Marina (LE), Italy, 22-26 June 1998.
(**) The authors of this paper have agreed to not receive the proofs for correction.

result showed the growth of anisotropy of flow field and the emergence of alternating bands of mean zonal current due to Rossby wave dynamics. Williams [7] took account of the exact spherical geometry in his numerical experiment on forced 2D turbulence, aiming at a reproduction of the zonal band structure of Jovian atmosphere. He obtained a clear band structure for a stochastic vorticity forcing. In his experiment, however, both longitudinal periodicity and equatorial symmetry were assumed in order to reduce the computational domain to 1/16 of the entire sphere.

Advancement of computing facilities in 1990s has enabled us to do these computations with much higher resolutions in full spherical geometry [8-11]. For high-rotation cases in the decaying turbulence experiments, Yoden and Yamada [8] found the emergence of a westward circumpolar vortex in high-latitudes. Such formation of a circumpolar vortex is also observed in the forced turbulence experiment [10] and in the laboratory experiment by Rhines [12]. However, there remains a concern about the initial condition used in the decaying turbulence experiments [8]: a large part of the energy is contained in large scales in which the linear rotation term dominates the nonlinear inertial term.

In this study, a further numerical experiment on the 2D decaying turbulence on a rotating sphere is done with a high-resolution model in order to see the pattern formation due to the real inverse cascade from small scales given by some appropriate initial conditions. Dependence of the energy spectrum and the flow pattern on the initial condition and the rotation rate is investigated systematically.

2. – Model and numerical procedure

Freely evolving 2D non-divergent flow on a rotating sphere is governed by the following vorticity equation:

$$\frac{\partial \omega}{\partial t} + \frac{1}{a^2} J(\psi, \omega) + \frac{2\Omega}{a^2} \frac{\partial \psi}{\partial \lambda} = (-1)^{p+1} \nu_{2p} \left(\Delta + \frac{2}{a^2} \right)^p \omega , \tag{1}$$

where $\psi(\lambda, \mu, t)$ is a streamfunction field, $\omega(\lambda, \mu, t)$ the vertical component of vorticity ($\equiv \Delta\psi$), λ the longitude, μ the sine latitude, t the time, $J(A, B)$ the horizontal Jacobian, Δ the horizontal Laplacian, a the radius of the sphere, Ω the rotation rate of the sphere. On the right-hand side hyper-viscosity of the order of p is assumed with a viscosity coefficient ν_{2p}. In the case of $\nu_{2p} = 0$, eq. (1) means the conservation of potential vorticity (or absolute vorticity in the present case) $q \equiv \omega + 2\Omega\mu$ following Lagrangian motion.

To construct a spectral model of eq. (1), we expand a dependent variable $\psi(\lambda, \mu, t)$ into a set of spherical harmonics and truncate it at the total wave number $N = 341$ (*i.e.*, triangular truncation T341): $\psi(\lambda, \mu, t) = \sum_{n=2}^{N} \sum_{m=-n}^{n} \psi_n^m(t) P_n^m(\mu) e^{im\lambda}$. A spectral transform method (see, *e.g.*, [13]) is used to compute the nonlinear Jacobian term; grids for the spectral transformation is 1024 (longitude) × 512 (latitude).

The time evolution of $\psi(\lambda, \mu, t)$ is computed from an initial random flow field, whose energy spectrum is given by

$$E(n, t = 0) = \frac{A n^5}{e^{-n/2}} \quad \text{or} \quad E(n, t = 0) = \frac{A n^{\gamma/2}}{(n + n_0)^\gamma} . \tag{2}$$

Here the energy density is given by $E(n, t) = (1/2)\, n(n+1) \sum_{m=-n}^{n} |\psi_n^m(t)|^2$. Each complex amplitude $\psi_n^m(t=0) = (-1)^m (\psi_n^{-m}(t=0))^*$ (where * denotes complex conjugate) is determined so that it has random amplitude and random phase under the above restriction. The former expression in (2) was assumed in [8] while the latter was used in [9]. A constant A is set so that the total kinetic energy is unity without dimension: $\mathcal{E}(t=0) = \sum_{n=2}^{N} E(n, t=0) = 1$.

Computations are done in a non-dimensional form. The radius of the sphere is taken as a length scale (L); $a = 1$ in the non-dimensional form. Advective time scale is adopted; the time scale (T) is equal to the length scale divided by a square root of mean kinetic energy (or velocity scale U). If we take a rough scaling for the atmosphere as $U \sim 10$ m/s and $L = 6 \times 10^6$ m, the time scale is $T \sim L/U = 6 \times 10^5$ s ~ 7 days. Six values of Ω are taken as an experimental parameter: 0, 25, 50, 100, 200 and 400. The sphere has $\Omega/(2\pi)$ rotations per unit time interval. If we take the above scaling, $\Omega = 50$ is close to the present rotation of the Earth.

The parameter values of the initial energy spectrum used in this study are listed in table I and the spectra are shown in fig. 1. Five vertical dashed lines in fig. 1 indicate the characteristic wave number $n_\beta \equiv \sqrt{\pi\Omega/(4U)} = \sqrt{\pi\Omega/(4\sqrt{2\mathcal{E}})}$ for each Ω; at the spatial scale n_β, the linear rotation term is comparable to the nonlinear Jacobian term in eq. (1). As stated in the introduction, the initial energy spectrum used in [8] (solid line) has much energy in large scales of $n < n_\beta$, where the linear term dominates. On the other hand, the spectral form used in [9], the latter in eq. (2), can limit the initial energy distribution near n_0 for a large value of γ. In this study we use five sets of initial conditions including the reexamination of [8] with higher resolution (denoted as yy1993); the control experiment (cpn050) is given by $(n_0, \gamma) = (50, 1000)$. The spectral peak of initial energy is located in much larger wave number than n_β in the three experimental sets with $n_0 = 50$ or 100 (cpn050, cpn100 and cpg100).

TABLE I. – *Description of the initial parameters for each experimental set and decay rates of total energy, $\mathcal{E}(t=5)/\mathcal{E}(t=0)$, and enstrophy, $\mathcal{Q}(t=5)/\mathcal{Q}(t=0)$. These ratios depending on the rotation rate Ω are listed in %, and are ensemble averages of 10 runs from the initial conditions made with different random numbers.*

Set name	yy1993 [8]		cpn010		cpn050 control exp.		cpn100		cpg100	
n_0	—		10		50		100		50	
γ	—		1000		1000		1000		100	
$\mathcal{Q}(t=0)$	180.0		111.7		2590.7		10262.1		2992.0	
Ω	$\mathcal{E}$[%]	$\mathcal{Q}$[%]	$\mathcal{E}$[%]	$\mathcal{Q}$[%]	$\mathcal{E}$[%]	$\mathcal{Q}$[%]	$\mathcal{E}$[%]	$\mathcal{Q}$[%]	$\mathcal{E}$[%]	$\mathcal{Q}$[%]
0	99.8	25.9	99.9	35.4	97.5	10.3	89.7	5.3	97.1	10.5
25	99.8	24.8	99.9	40.6	97.4	7.6	89.6	4.3	97.0	7.8
50	99.8	29.9	99.9	51.3	97.3	5.5	89.5	3.1	96.9	5.6
100	99.9	40.8	100.0	67.9	97.3	4.2	89.3	1.8	96.9	4.0
200	99.9	53.3	100.0	78.4	97.3	5.1	89.3	1.4	96.9	4.6
400	99.9	65.3	100.0	87.7	97.4	7.6	89.3	1.9	96.9	6.5

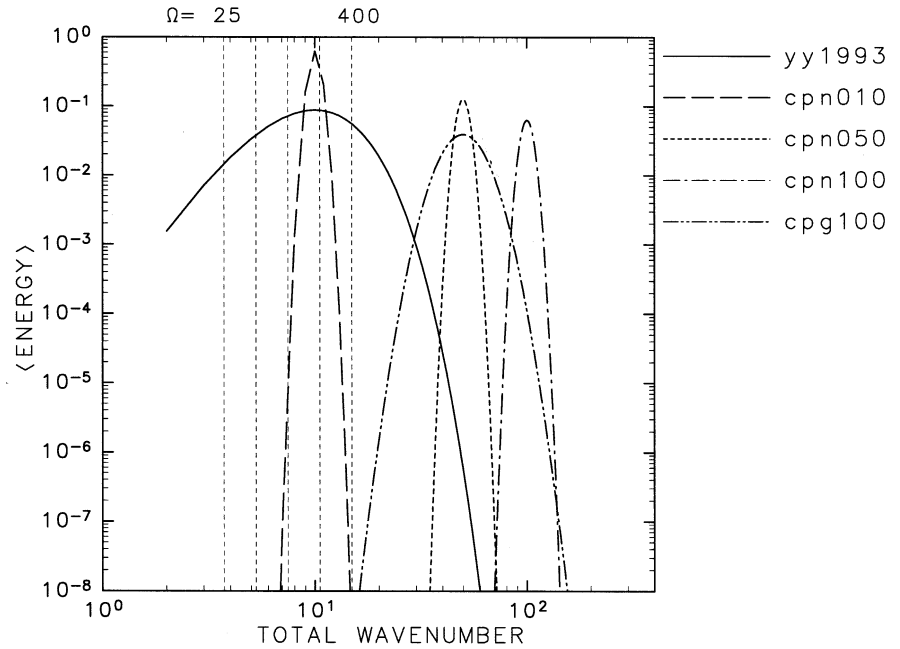

Fig. 1. – Five initial energy spectra used in this study. The spectral form is given by eq. (2) and the parameter values are listed in table I. The five vertical dashed lines indicate the characteristic wave number $n_\beta = \sqrt{\pi\Omega/(4\sqrt{2})}$.

The hyper-viscosity is set with $p = 8$ and $\nu_{2p} = 1 \times 10^{-38}$. Ten initial conditions are made with different random numbers for each experimental set, and time evolutions from these are computed until $t = 5$ by the fourth-order Runge-Kutta method with the time increment of $\Delta t = 1 \times 10^{-3}$. All of the computations are done in double precision.

3. – Results

3·1. *Energy and enstrophy.* – Figure 2 shows time variations of the total energy $\mathcal{E}(t)$, the total enstrophy $\mathcal{Q}(t) \equiv (1/2) \sum_{n=2}^{N} n^2(n+1)^2 \sum_{m=-n}^{n} |\psi_n^m(t)|^2$, and the enstrophy dissipation rate $\eta(t) = -\mathrm{d}\mathcal{Q}/\mathrm{d}t$ for the six values of the rotation rate Ω in the control experiment. Time variations of these quantities are not very sensitive to Ω. The total energy dissipates about 2% by $t = 1$ and it is nearly conservative afterward. On the other hand, the total enstrophy has a maximum dissipation rate around $t \sim 0.2$ and decays as $\mathcal{Q}(t) \propto t^{-1}$ after that time.

Decay rates of the total energy and the total enstrophy for the integration period are listed in table I for the five experimental sets. The energy is almost conserved for the cases in which the spectral peak of the initial energy is located in a low wave number (yy1993 and cpn010), while the energy decay is about 10% when the spectral peak is at $n = 100$ (cpn100). On the other hand, the enstrophy decay is dependent on the initial energy spectra. The decay rate is smaller if the spectral peak is at a lower wave number, particularly for the cases of large Ω.

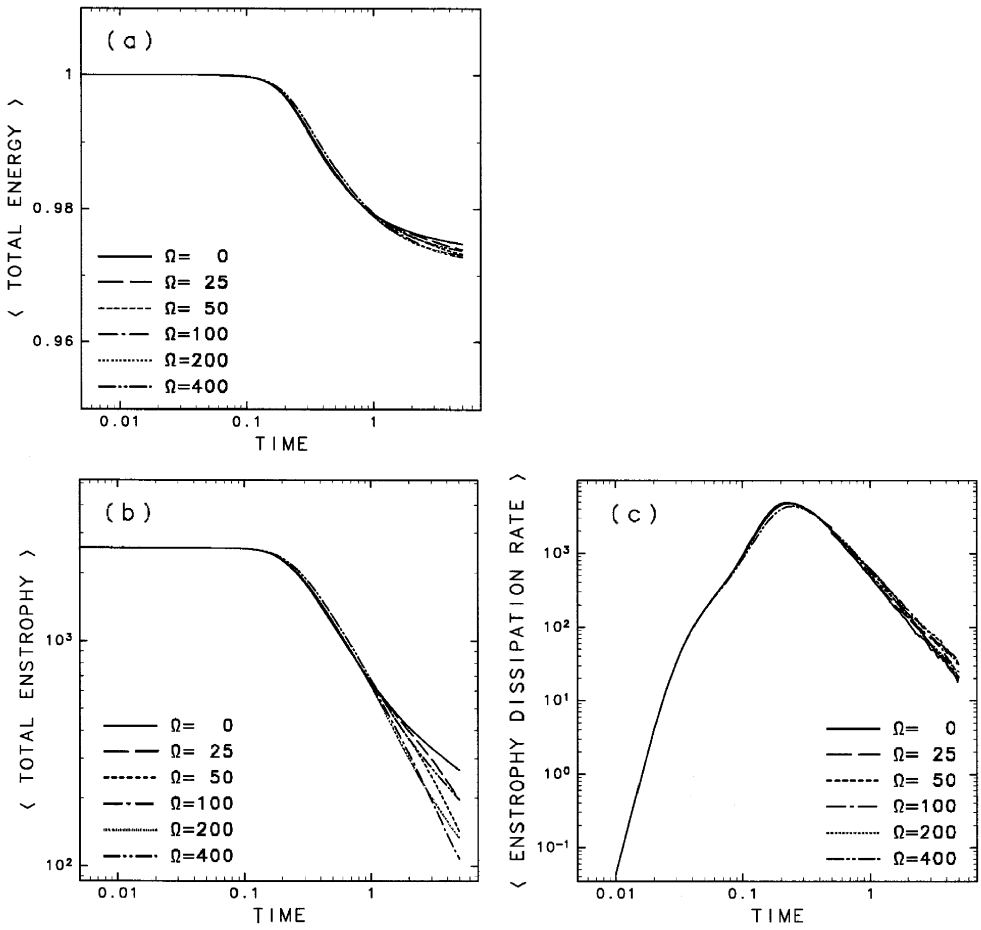

Fig. 2. – Time variation of total energy (a), total enstrophy (b), and enstrophy dissipation rate (c) for six values of Ω in the control experiment, cpn050. Ensemble average of 10 runs.

Time evolution of the energy spectrum $E(n, t)$ is dependent on the initial spectrum and the rotation rate as shown in fig. 3(a-e). In the non-rotational cases ($\Omega = 0$; solid lines), a slope close to n^{-3} appears if the initial spectral peak is at a low wave number (cpn010, yy1993), but any clear power law as in the forced turbulence [11] is not obtained for the sets of cpn050, cpn100 and cpg100 even though there are cascading ranges in both sides. On the other hand, another slope of the energy spectrum appears in rotational cases. Dashed lines in fig. 3(a-e) show a power law close to n^{-4} in a wide range for the high-rotation case of $\Omega = 400$. Figure 3(f) is the direct confirmation of the n^{-4} power law; cpn010 is the clearest set showing this law over one order of n. Note that this range extends to low wave numbers less than n_β.

In rotational cases, anisotropy due to the rotation appears in the flow field, and it is worthwhile looking at a 2D energy spectrum with zonal wave number m and total wave number n. The energy density of small m is dominant in the range of $n < n_\beta$ while the energy is very small in an airfoil-shaped region at the lower edge in the wave number

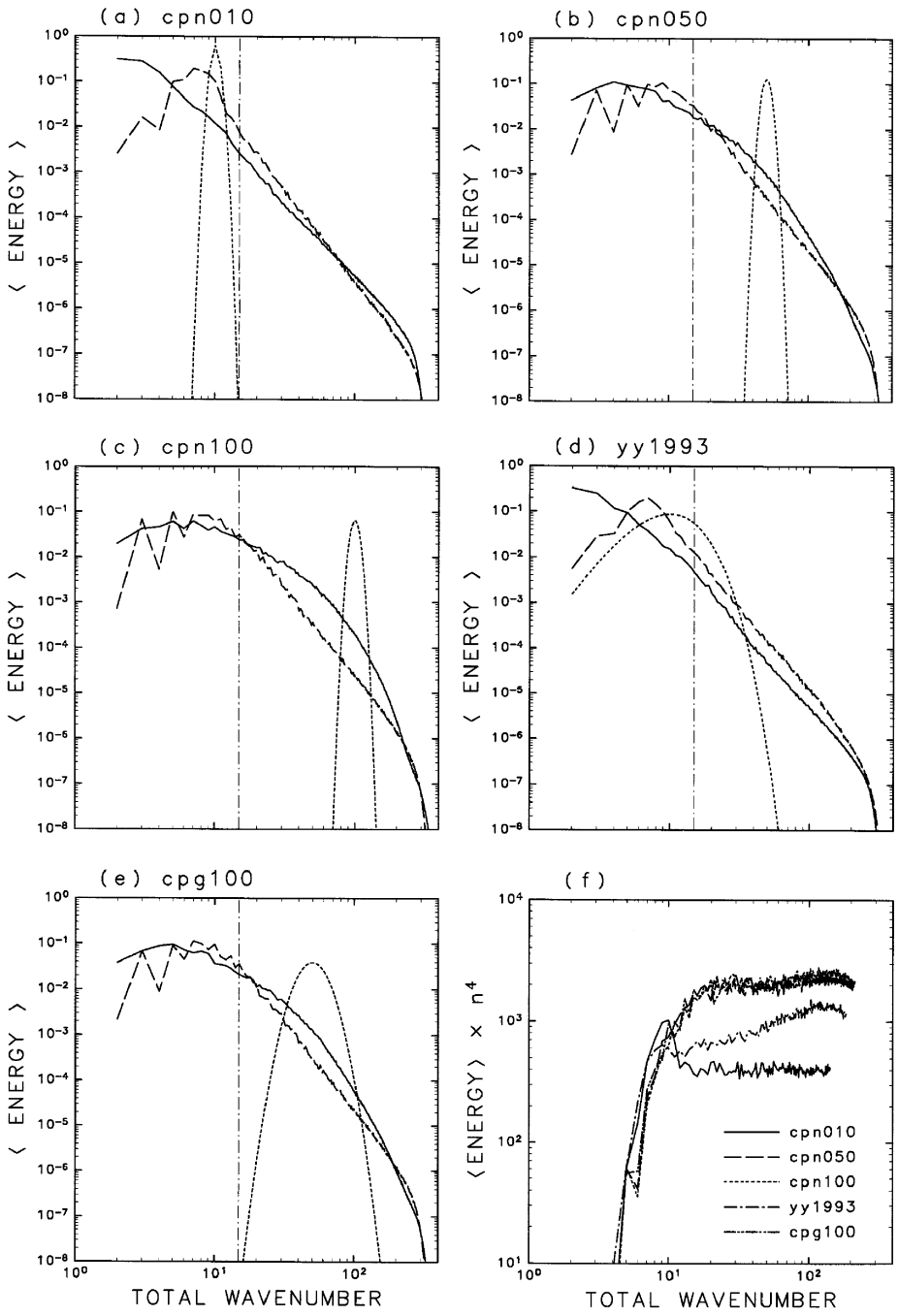

Fig. 3. – (a)-(e) Energy spectra for five experimental sets at $t = 0$ (dotted line) and at $t = 5$ (solid line for $\Omega = 0$ and dashed line for $\Omega = 400$). The vertical dash-dotted line indicates the characteristic wave number n_β for $\Omega = 400$. (f) $E(n) \times n^4$ at $t = 5$ for five experimental sets in the case of $\Omega = 400$.

space (m, n) as found in the forced turbulence experiments [11, 14] (not shown). The existence of such a small energy region is qualitatively explained by the analogy of a dumbbell region obtained in the β-plane experiment by Vallis and Multrad [15]. Anisotropic distribution of the energy is also found in the high total-wave number region $n > n_\beta$; energy is confined in the region of small zonal wave number m. This should be directly related to the anisotropy in the low total-wave number region through the non-linear Jacobian term.

3·2. *Flow fields.* – Time evolution of the flow field can be viewed by movies of the potential vorticity and the vorticity fields. (A copy of the VHS video is available from the authors.) Figure 4 shows some snapshots of the vorticity field for the non-rotational case in the control experiment. The initial vorticity field is homogeneous and isotropic due to the random initial condition. At $t = 1$, high-gradient, filamentary structures are created, which are indicative of the dissipation of enstrophy in small scales, and eventually isolated coherent vortices emerge as in the planar 2D turbulence [5] through mergers of vortices with the same sign of vorticity.

Time evolution of the flow field is largely dependent on the rotation rate Ω. Figure 5 is an example to show the dependence of vorticity field at $t = 5$ evolved from the same initial condition shown in fig. 4 (left) on the rotation rate. In the non-rotational case (left), the number of the coherent vortices decreases from $t = 2$ shown in fig. 4 (right) owing to their mergers, and filamentary structures dim out after large enstrophy dissipation. In the high-rotation case of $\Omega = 400$ (right), on the other hand, the vorticity field is not isotropic but shows zonally elongated structures. The zonal mean zonal angular momentum shows the emergence of westward circumpolar vortex, particularly in the southern hemisphere for this run, as well as zonal band structures in mid and low latitudes. Movies of the (potential) vorticity field for rotational cases clearly show westward propagation of the disturbance as «Rossby waves» generated by the upward energy cascade. Remember that the energy spectrum with n^{-4} power law indicated by the dashed line in fig. 3(b) should be related to the vorticity distribution shown in fig. 5 (right).

If we look at the time evolution of the zonal mean zonal angular momentum (not shown), we can reconfirm the formation of westward circumpolar vortex in high

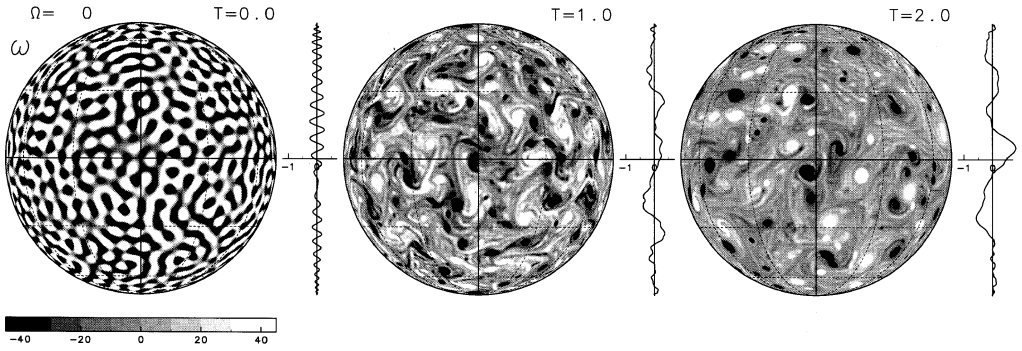

Fig. 4. – Time evolution of the vorticity field for $\Omega = 0$ in the control experiment: (left) $t = 0$, (center) $t = 1$, and (right) $t = 2$. Orthographic projection from $\lambda = 0°$, $\phi = 0°$ is used and lines of meridians and parallels are drawn for every 30°. The solid line on the right side of each panel shows the zonal mean zonal angular momentum as a function of sine latitude.

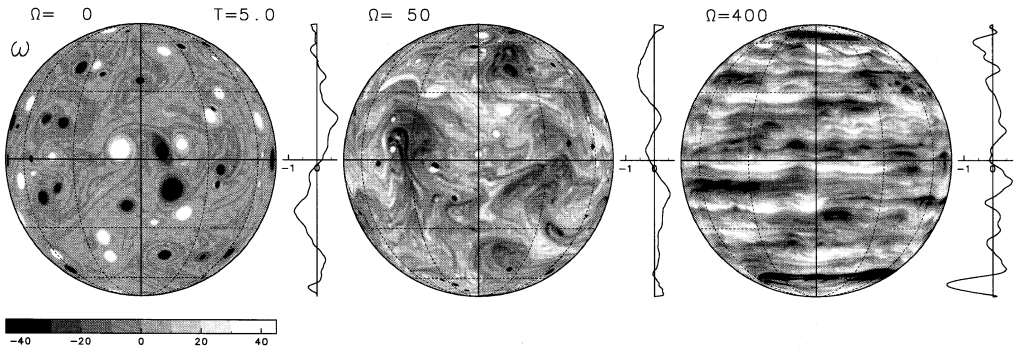

Fig. 5. – Vorticity field at $t = 5$ depending on the rotation rate in the control experiment: (left) $\Omega = 0$, (center) $\Omega = 50$, and (right) $\Omega = 400$. The same projection as in fig. 4 is used. The solid line on the right side of each panel shows the zonal mean zonal angular momentum as a function of sine latitude.

latitudes and zonal band structure of alternating mean zonal jets in mid and low latitudes for high-rotation cases. These structures are discernible from such an early stage of $t \sim 0.5$ and their latitudinal positions are hardly changed with time. Generally,

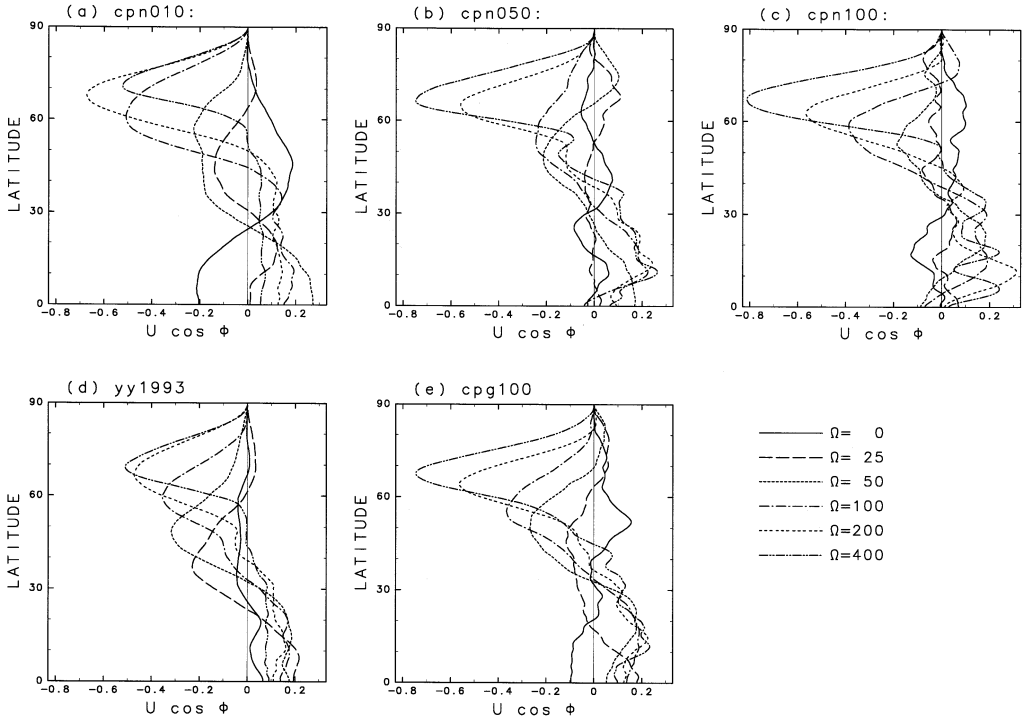

Fig. 6. – Dependence of zonal mean zonal angular momentum on the rotation rate Ω for the five experimental sets (a)-(e). Ensemble average of 2×10 runs is shown under the assumption of equatorial symmetry.

the number of the jets increases while the width of them decreases, as the rotation rate Ω increases.

Figure 6 shows the dependence of the zonal mean zonal angular momentum at $t = 5$ on Ω for the five experimental sets (a-e). The formation of the westward circumpolar vortex for large Ω is a robust result independent of the choice of the initial energy spectrum; in these experiments, the intensity of the westward vortex becomes large and its maximum position shifts into higher latitudes as Ω increases. Note that the westward vortex for $\Omega = 400$ is stronger for larger n_0 (b, c and e). As a result of the ensemble average, eastward flow appears in low latitudes for large Ω owing to the conservation law of total angular momentum. However, each realization shows a zonal band structure in mid and low latitudes. The ensemble average masks the band structure because the latitudinal position of the jets is dependent on each realization.

4. – Concluding remarks

A series of numerical experiments on the two-dimensional (2D) decaying turbulence on a rotating sphere was performed with a high-resolution spectral model of T341 truncation (1024×512 transformation grids). Time integrations were repeatedly done from 5 initial energy spectra with 10 different random vorticity fields by taking the rotation rate of the sphere with 6 values from zero to a large one (*i.e.*, totally 300 integrations were done). The main results are as follows:

1. One-dimensional energy spectra for high-rotation cases show a power law of $E(n) \propto n^{-4}$ (fig. 3) in contrast to the well-known non-rotational cases in which the spectrum does not show clear power law.

2. 2D energy spectrum with zonal- and total-wave number space shows anisotropy due to the rotation effect of the sphere. An airfoil shape with very small energy density appears in low total-wave number region. Anisotropic distribution of the energy is also found in the high total-wave number region.

3. The flow field becomes anisotropic owing to the effect of rotation. A westward circumpolar vortex appears in high latitudes and zonal band structures of alternating mean zonal jets appear in mid and low latitudes for high-rotation cases.

4. The formation of the westward circumpolar vortex is a robust feature of the 2D decaying turbulence on a rotating sphere and insensitive to the choice of the initial energy spectrum.

5. The zonal band structures are discernible from an early stage of the time evolution, and once established their latitudinal positions are hardly changed with time. As the rotation rate increases, the number of the jets increases while the width of them decreases.

The dynamics of the formation of the westward circumpolar vortex is not thoroughly understood yet. Rhines [12, 16] pointed out the importance of the homogenization of potential vorticity in high latitudes: "stirring of potential vorticity leads to the predictable polar anticyclone, almost regardless of the detailed nature of the Rossby waves or geostrophic turbulence." However, fig. 6 shows the emergence of eastward flow in mid and low latitudes on average, which is indicative of the angular momentum transport even from the low latitudes. The dynamical role of Rossby waves in the formation of the circumpolar vortex is under investigation within the framework

of a weakly nonlinear wave-zonal flow interaction theory and will be reported elsewhere [17].

* * *

The GFD-DENNOU Library [18] was used for drawing the figures. Numerical calculation was done on VPP500/15 at the Data Processing Center, Kyoto University. This work was supported in part by the Grant-in-Aid for Scientific Research of the Ministry of Education, Science, Sports and Culture of Japan and by the Grant-in-Aid for the Research for the Future Program "Computational Science and Engineering" of the Japan Society for the Promotion of Science.

REFERENCES

[1] KRAICHNAN R. H., *Phys. Fluids*, **10** (1967) 1417.
[2] LEITH C. E., *Phys. Fluids*, **11** (1968) 671.
[3] BATCHELOR G. K., *Phys. Fluids Suppl.*, **II** (1969) 233.
[4] BORUE V., *Phys. Rev. Lett.*, **71** (1993) 3967.
[5] MCWILLIAMS J. C., *J. Fluid Mech.*, **146** (1984) 21.
[6] RHINES P. B., *J. Fluid Mech.*, **69** (1975) 417.
[7] WILLIAMS G. P., *J. Atmos. Sci.*, **35** (1978) 1399.
[8] YODEN S. and YAMADA M., *J. Atmos. Sci.*, **50** (1993) 631.
[9] CHO, J. Y.-K. and POLVANI L. M., *Phys. Fluids*, **8** (1996) 1531.
[10] NOZAWA T. and YODEN S., *Phys. Fluids*, **9** (1997) 2081.
[11] NOZAWA T. and YODEN S., *Phys. Fluids*, **9** (1997) 3834.
[12] RHINES P. B., http://www.ocean.washington.edu/people/staff/lindahl/rossby.html (1998).
[13] WASHINGTON W. M. and PARKINSON C. L., in *An Introduction to Three-dimensional Climate Modeling* (University Science Books, Mill Valley) 1986, pp. 161-208.
[14] HUANG H. P. and ROBINSON W. A., *J. Atmos. Sci.*, **55** (1998) 611.
[15] VALLIS G. K. and MALTRUD M. E., *J. Phys. Oceanogr.*, **23** (1993) 1346.
[16] RHINES P. B., *Chaos*, **4** (1994) 313.
[17] HAYASHI Y.-Y., ISHIOKA K., YAMADA M. and YODEN S., to be published in *Proceedings of the IUTAM/IUGG Symposium on "Developments in Geophysical Turbulence", Boulder 1998*, edited by R. M. KERR and Y. KIMURA.
[18] SGKS GROUP, http://www.gfd-dennou.org/library/dcl/, DCL-5.1 (in Japanese) 1995.